J|A|C|S
ARTICLES
Published on Web 06/08/2002

Structural Control in Thin Layers of Poly(*p*-phenyleneethynylene)s: Photophysical Studies of Langmuir and Langmuir−Blodgett Films

Jinsang Kim,[†,‡] Igor A. Levitsky,[†] D. Tyler McQuade,[†] and Timothy M. Swager*[,†]

Contribution from the Department of Chemistry and Department of Materials Science and Engineering, Massachusetts Institute of Technology, Cambridge, Massachusetts 02139

Received January 10, 2002

Abstract: We present the relationship between the spatial arrangement and the photophysical properties of fluorescent polymers in thin films with controlled structures. Eight surfactant poly(*p*-phenyleneethynylene)s were designed and studied. These detailed studies of the behavior of the polymers at the air−water interface, and of the photophysical properties of their transferred LB films, revealed key structure−property relationships. Some of the polymers displayed π-aggregates that are characteristic of an edge-on structure at the air−water interface. Monolayer LB films of these polymers showed greatly reduced quantum yields relative to solution values. Other polymers exhibited a highly emissive face-on structure at the air−water interface, and did not form π-aggregates. The combination of pressure−area isotherms and the surface pressure dependent in situ UV−vis spectra of the polymers at the air−water interface revealed different behavioral details. In addition, the UV−vis spectra, fluorescence spectra, and quantum yields of the LB films provide design principles for making highly emissive films.

Introduction

A comprehensive understanding of the electronic states of conjugated polymers is pivotal to the continued development of these materials. In general, the electronic structure of isolated chains is well understood and is readily approximated by oligomeric compounds due to the limited effective chromophore dimensions in these materials. However, there is invariably electronic coupling between polymer chains, and these secondary interactions often dominate a material's redox potential, band gap, fluorescence efficiency, and electrical energy transport.[1] The transport properties of conjugated polymers, their most interesting feature, are extremely sensitive to interpolymer interactions. This fact follows from the necessity of transfer of charge or excitations between polymer chains.

Much of the technological promise of conjugated polymers rests on their emissive properties. Applications include electroluminescent displays,[2] organic lasers,[3] and sensors.[4] Our group's interest in conjugated polymers for the amplification of sensory signals[4a] requires optimization of their transport properties. Within this framework, many factors need be considered. Among these are the polymer's absorption and emission spectra, degree of organization, bandwidth, band gap, emission quantum yield and lifetimes, and energy transport dynamics. The evolution of electronic structure from the constituent chromophores of a polymer is reasonably well understood; however, interchain interactions have less predictable consequences. Nevertheless, strong electronic coupling between polymer chains has the prospect to increase intermolecular energy transfer. Most often strong interpolymer interactions give rise to distinct red shifts in the absorption spectra and generally produce less emissive (quenched) materials.[5,6] It is generally assumed that polymers prefer to organize with cofacial π interactions, and structural studies support this fact.[7−9] However, the detailed role of interpolymer interactions on luminescent polymers' absorption and emission properties has not been systematically studied due to the difficulty in controlling interpolymer arrangement. Greater understanding of chain−chain interactions in conjugated polymers is clearly necessary

* To whom correspondence should be addressed. E-mail: tswager@mit.edu.
† Department of Chemistry.
‡ Department of Materials Science and Engineering.

(1) (a) Cornil, J.; Heeger, A. J.; Bredas, J. L. *Chem. Phys. Lett*. **1997**, *272*, 463. (b) Cornil, J.; dos Santos, D. A.; Crispin, X.; Silbey, R.; Bredas, J. L. *J. Am. Chem. Soc*. **1998**, *120*, 1289. (c) Bredas, J. L.; Cornil, J.; Beljonne, D.; dos Santos, D. A.; Shuai, Z. *Acc. Chem. Res*. **1999**, *32*, 267.
(2) Friend, R. H.; Gymer, R. W.; Holmes, A. B.; Burroughes, J. H.; Marks, R. N.; Taliani, C.; Bradley, D. D. C.; dos Santos, D. A.; Bredas, J. L.; Logdlund, M.; Salaneck, W. R. *Nature* **1999**, *397*, 121.
(3) (a) Hide, F.; Schwartz, B. J.; Diazgarcia, M. A.; Heeger, A. J. *Chem. Phys. Lett*. **1996**, *256*, 424. (b) Hide, F.; Diazgarcia, M. A.; Schwartz, B. J.; Anderson, M. R.; Pei, Q. B.; Heeger, A. J. *Science* **1996**, *273*, 1833.
(4) (a) Swager, T. M. *Acc. Chem. Res.* **1998**, *31*, 201. (b) Yang, J. S.; Swager, T. M. *J. Am. Chem. Soc*. **1998**, *120*, 5321. (c) Yang, J. S.; Swager, T. M. *J. Am. Chem. Soc.* **1998**, *120*, 11864. (d) Kim, J.; McQuade, D. T.; McHugh, S. K.; Swager, T. M. *Angew. Chem., Int. Ed.* **2000**, *39*, 3868. (e) McQuade, D. T.; Pullen, A. E.; Swager, T. M. *Chem. Rev.* **2000**, *100*, 2537.
(5) (a) Jenekhe, S. A.; Osaheni, J. A. *Chem. Mater*. **1994**, *6*, 1906. (b) Jenekhe, S. A.; Osaheni, J. A. *Science* **1994**, *265*, 765. (c) Jenekhe, S. A. *Adv. Mater*. **1995**, *7*, 309. (d) Osaheni, J. A.; Jenekhe, S. A. *J. Am. Chem. Soc.* **1995**, *117*, 7389.
(6) McQuade, D. T.; Kim, J.; Swager, T. M. *J. Am. Chem. Soc*. **2000**, *122*, 5885.
(7) Weder, C.; Wrighton, M. S. *Macromolecules* **1996**, *29*, 5157.
(8) Li, H.; Powell, D. R.; Hayashi, R. K.; West, R. *Macromolecules* **1998**, *31*, 52.
(9) (a) Halkyard, C. E.; Rampey, M. E.; Kloppenburg, L.; Studer-Martinez, S. L.; Bunz, U. H. F. *Macromolecules* **1998**, *31*, 8655. (b) Levitus, M.; Schmieder, K.; Ricks, H.; Shimizu, K. D.; Bunz, U. H. F.; Garcia-Garibay, M. A. *J. Am. Chem. Soc.* **2001**, *123*, 4259−4265.

10.1021/ja0200600 CCC: $22.00

to reveal under which circumstances these interactions will lead to emissive[10] or quenched π-aggregated materials. Added fidelity is required to understand the circumstances, wherein proximal chain−chain interactions can lead to excited-state aggregation and produce strong exciplex emissions.

Investigations are best performed when organized assemblies of polymers can be prepared with predictable or manipulatable conformations and intermolecular interactions. In this regard, combination of surfactant polymer design and the Langmuir−Blodgett (LB) technique[11] is very useful. We have recently synthesized surfactant poly(*p*-phenyleneethynylene)s (PPEs) and used a LB trough to create spatially well-defined Langmuir films.[12] In these previous studies, we identified three specific geometries. The first involves cofacial organization of the π-plane with the air−water interface, referred to as the face-on structure. The second geometry wherein the plane of the conjugated π-system lies normal to the air−water interface is referred to as the edge-on structure. The third one is the zipper structure, alternating face-on and edge-on structures. In our earlier systems,[13] we determined that the face-on structure provided a dynamic phase with liquid crystalline characteristics at the air−water interface and was readily transferred to a support to give highly aligned materials. Chain alignment plays an important role in Förster energy transfer since those processes are highly dependent upon the coincidence of transition dipoles between donors and acceptor chromophores.[14,15] The edge-on structure gives crystalline aggregates on the LB trough that are not amendable to organization by flow fields or anisotropic compression. Nevertheless, these edge-on structures represent an ideal situation for the organization of materials into well-defined cofacial π-aggregated structures. In both cases, the structures can be manipulated by applying pressure with the LB trough. This exquisite structural control, as well as the ability to transfer materials monolayer by monolayer, provides the most controlled preparation of conjugated polymer assemblies to date. The LB method also creates an extraordinary venue for investigations directed at interfacing conjugated polymers with water-soluble elements, and thereby establishes a firm foundation from which to construct novel biosensory materials.

Herein we describe studies of PPEs designed to have specific surfactant characteristics. We have broadened the scope of structures that display edge-on or face-on structures and have discovered conditions wherein the applied pressure can manipulate the polymer chromophores at the air−water interface. We have also systematically studied how interpolymer interactions affect the fluorescent polymers' ground and excited states in structurally defined monolayer films and solid solutions of the polymers in PMMA. The approaches described herein have broad applicability to a range of conjugated polymer structures and illustrate the utility of LB techniques for the elucidation of the structure−property relationships in conjugated polymers.

Results and Discussion

Building upon our designs of PPEs that adopt face-on or edge-on geometries at the air−water interface,[12,13] eight polymers

Chart 1

Edge-on Structure (1-3)

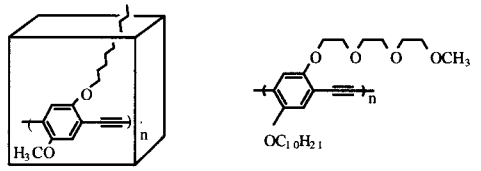

1 Mn =13 900 PDI = 3.2 **2** Mn = 55 900 PDI = 2.9

Face-on Structure (4-8)

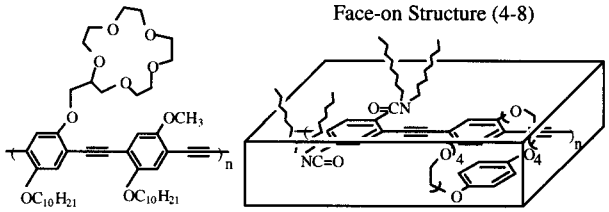

3 Mn = 19 600 PDI = 2.5 **4** Mn = 81 200 PDI = 3.4

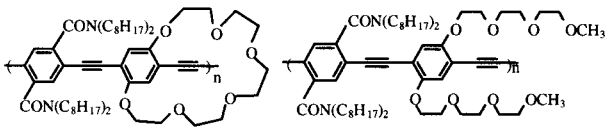

5 Mn = 56 000 PDI = 2.5 **6** Mn = 23 600 PDI = 2.4

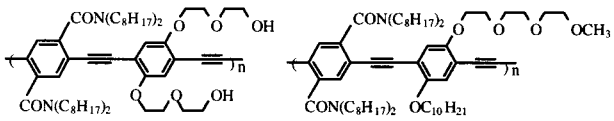

7 Mn = 51 600 PDI = 3.8 **8** Mn = 16 700 PDI = 2.4

were investigated (Chart 1). Palladium-catalyzed cross-coupling methods figure prominently into the synthesis of these polymers.[16,17] The preparation of polymers **1**, **3**, **4**, and **6** was reported elsewhere.[4d,12,13,23] Polymers **2** and **8** were synthesized as described in eq 1. The preparation of **9** was reported elsewhere.[12] Monomer **9** was further reacted with 1-((triethylene glycol monomethyl ether)oxy)-4-decyloxy-2,5-diiodobenzene or 1,4-bis(*N*,*N*-dioctylcarbamoyl)-2,5-diiodobenzene to produce polymers **2** and **8**, respectively.

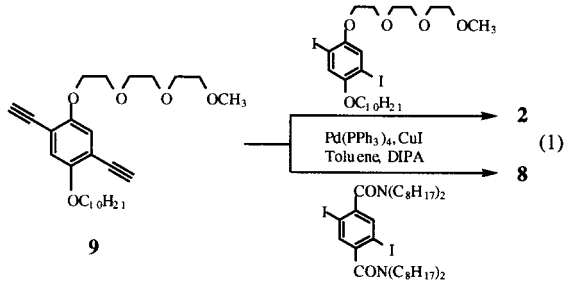

9 (1)

Polymer **5** was synthesized from the palladium coupling reaction of **10** with 1,4-bis(*N*,*N*-dioctylcarbamoyl)-2,5-diiodobenzene (eq 2). Pentaethylene glycol ditosylate was reacted with 1,4-diiodo-2,5-dihydroxybenzene under standard Williamson ether conditions, followed by palladium-catalyzed coupling (trimethylsilyl)acetylene and deprotection to give 2,5-diethynyl-*p*-phenylene-20-crown-6 (**10**).

(10) Deans, R.; Kim, J.; Machacek, M.; Swager, T. M. *J. Am. Chem. Soc.* **2000**, *122*, 8565.
(11) Wegner, G. *Thin Solid Films* **1992**, *216*, 105.
(12) Kim, J.; Swager, T. M. *Nature* **2001**, *411*, 1030.
(13) Kim, J.; McHugh, S. K.; Swager, T. M. *Macromolecules* **1999**, *32*, 1500.
(14) Förster, T. *Ann. Phys.* **1948**, *2*, 55.
(15) Levitsky, I. A.; Kim, J.; Swager, T. M. *J. Am. Chem. Soc.* **1999**, *121*, 1466.
(16) Sonogashira, K.; Tohda, Y.; Hagihara, N. *Tetrahedron Lett.* **1975**, 4467.
(17) Swager, T. M.; Gil, C. J.; Wrighton, M. S. *J. Phys. Chem.* **1995**, *99*, 4886.

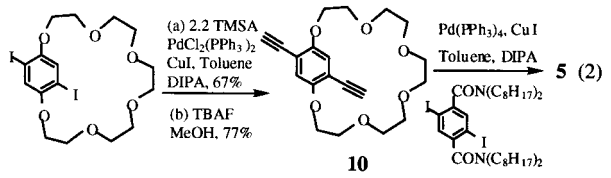

As shown in eq 3, polymer **7** was synthesized from the coupling reaction of **11** with 1,4-bis(*N*,*N*-dioctylcarbamoyl)-2,5-diiodobenzene. 1,4-Bis[2-(2-hydroxyethoxy)ethoxy]-2,5-diiodobenzene was subjected to palladium-catalyzed coupling (trimethylsilyl)acetylene followed by deprotection to give 1,4-bis-[2-(2-hydroxyethoxy)ethoxy]-2,5-diethynylbenzene (**11**).

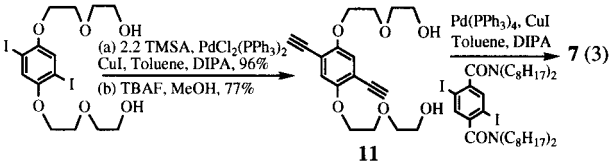

Our designs allowed us to control the interpolymer arrangement and intrapolymer conformations at the air−water interface. Polymers **1**, **2**, and **3** have the edge-on structure at the air−water interface due to the presence of hydrophilic groups on only one side of each phenyl ring. Polymers **4**−**8** comprise a second group that have a face-on structure with a symmetric para disposition of side groups. The edge-on polymers have π-aggregation between polymer chains, but the face-on polymers do not.

The pressure−area (PA) isotherms of polymers **1**−**8** at the air−water interface confirm our assertions of the polymers' orientational preferences (Figure 1). The extrapolated areas per phenyleneethynylene group for polymers **1**, **2**, and **3** range from 32 to 37 Å^2.[18] Combining this area with one phenyleneethynylene unit length of 7 Å provides the average distance between polymer main chains of 4.6 to 4.9 Å for an edge-on structure. In contrast, polymers **4**−**8** exhibit areas of 175−230 Å^2 per each repeating unit that has two phenyleneethynylene units. Considering a face-on structure, we calculated a distance between adjacent main chain acetylene carbons of 12.1−16.4 Å. The sustainable maximum pressure above which monolayers fold into multilayers was approximately 40 mN/m for the edge-on polymers, a value 10 mN/m higher than those for the face-on polymers. It is intuitive that the edge-on structure, which provides a larger contact area between polymers, sustains a larger surface pressure than does the face-on organization. One would expect a similar behavior for macroscopic objects such as boards organized in two dimensions with a vertical (edge-on) or horizontal (face-on) structure. The steep slopes of the P−A isotherms of the edge-on polymers also indicate the expected low compressibility associated with this structure.

The difference between extrapolated area per repeating unit of **4** and **5**, 210 and 175 Å^2, respectively, provides insight into the arrangement of adjacent polymers at the air−water interface. Polymer **5** has the same 1,4-bis(*N*,*N*-dioctylcarbamoyl)phenyl group as **4** but a smaller macrocycle in its repeating unit. To achieve the minimum area arrangement in two dimensions, the bulkier 1,4-bis(*N*,*N*-dioctylcarbamoyl)phenyl repeating units likely are positioned next to a macrocycle containing units of adjacent chains to give an interdigitated structure.

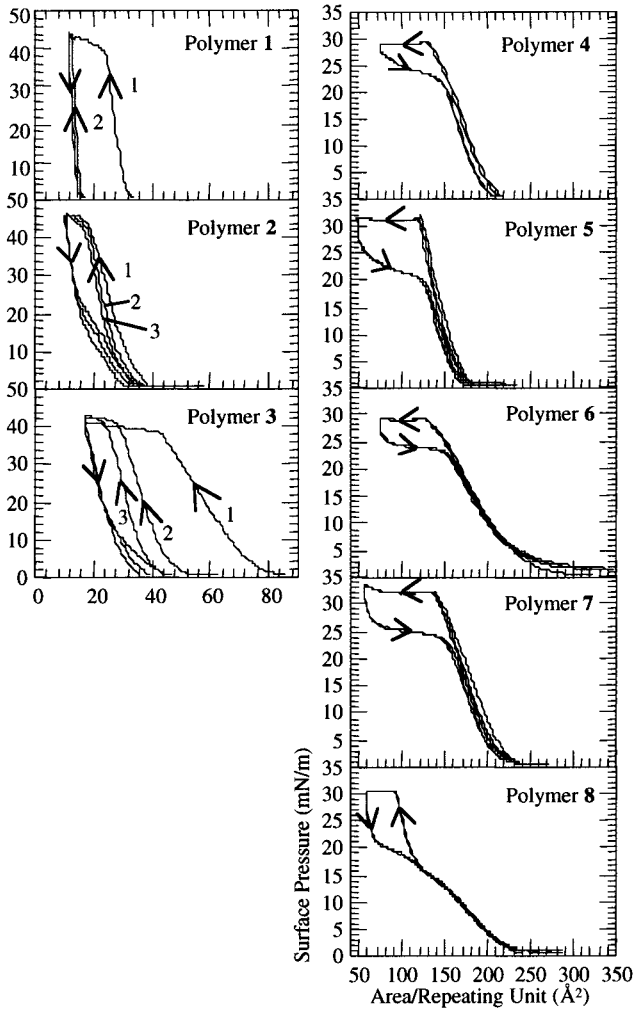

Figure 1. Pressure−area isotherms of polymers.

The area per repeating units at which the polymers fold into multilayers is similar for polymers **4**−**7** (125−140 Å^2) but is much smaller for polymer **8** (90 Å^2), indicating more compressible nature of polymer **8**. An explanation is that the main chain phenyl rings of polymers **4**−**7** maintain a face-on structure until the monolayers fold into multilayers at 30 mN/m. However, polymer **8** undergoes a two-stage transformation. It begins in a face-on structure, but as it is compressed, the orientation of the 1-((triethylene glycol monomethyl ether)oxy)-4-decyloxyphenylene groups, which have surfactant characteristics, rotates to an edge-on structure.[12] The reluctance of the hydrophobic repeating group to adapt an edge-on structure produces an intermediate structure with alternating edge-on and face-on residues, which we refer to as a zipper structure as shown in Scheme 1.[12] Therefore, the first slope of **8**'s PA isotherm is smaller than those of the other face-on polymers. After an intermediate (ca. 16 mN/m) transition point, the polymers become less compressible with a steep slope until the monolayers fold into multilayers at 30 mN/m. We synthesized two different molecular weights of polymer **8**. One is the polymer with a lower molecular weight (M_n = 16 700) that is used for this contribution, and the other one we used in previous studies[12] has a higher molecular weight (M_n = 293 000). The lower molecular polymer shows less featured PA isotherm and lower

(18) The extrapolated area per repeating unit for polymer **3** was divided by 2 because there are two phenyleneethynylene groups on the repeating unit.

Scheme 1

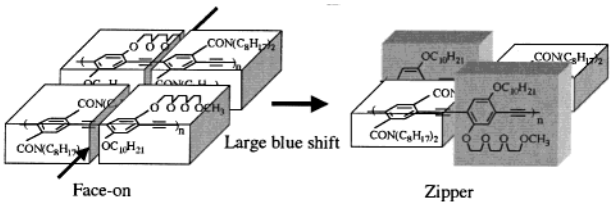

maximum surface pressure (30 vs 37 mN/m) as compared to the higher molecular weight one because chain ends would disrupt the interlocking zipper structure. Likewise, we previously reported[12] that diacetylene defects in this structure destroy long-range registry between neighboring polymer chains and the presence of these groups prevents well-defined phase transitions.

The in situ UV−vis spectra versus surface pressure of the Langmuir polymer films strongly support the above PA isotherm-based explanation of the arrangements and conformations of the polymers. At the air−water interface, the face-on polymers have a flat geometry with a maximum conjugation length. The in situ UV−vis spectra of the face-on polymers at the air−water interface are red-shifted about 30 nm from these in solution, showing surface-induced conjugation length increases (compare Figures 2 and 3).[12,19−21] The absorption λ_{max} of polymers **4**−**7** is blue-shifted, and the shape of the spectra becomes less structured during the compression (Figure 2). This disturbance of the $\pi-\pi$ conjugation system is likely due to interpolymer steric interactions that create a more heterogeneous distribution of conjugation lengths. The case of polymer **8** is again different and is characteristic of a zipper organization where the absorption λ_{max} blue shifts by 37 nm relative to its initial uncompressed face-on structure. The in situ absorption λ_{max} of the edge-on polymers at the air−water interface is essentially constant during compression because there is no perturbation of the $\pi-\pi$ conjugation system due to a highly packed crystalline monolayer structure (Figure 2).

As described above, we have demonstrated control of intramolecular conformation and interpolymer arrangement of the fluorescent polymers by rational surfactant designs and the types of interactions that occur with increased surface pressure. In the following section, the nature of each peak of the in situ UV−vis spectra, the red-shifted absorption peaks of transferred LB films, and corresponding fluorescent spectra are elaborated.

Interpolymer Effects on the Ground and Excited States. Both the edge-on and the face-on Langmuir films were transferred onto hydrophobic and hydrophilic substrates. The transfer ratios at a surface pressure of 20 mN/m for polymers **1**−**3**, displaying an edge-on structure, were quantitative (>95%) for both upstrokes and downstrokes. However, the transfer ratios of the downstrokes for polymers **4**−**8** depended on the area per repeating unit rather than on the surface pressure. For example, the second downstroke transfer ratios of polymer **4** at 18 mN/m were negligible (<10%). In contrast, the second downstroke for polymer **5** at the same surface pressure gave an 80% transfer ratio. The area/repeating unit of polymer **4** at 18 mN/m is 175 Å^2, while that of polymer **5** is 145 Å^2. Therefore, at 18 mN/m the hydrophobic octyl side chains of polymer **5** are more compressed than those of polymer **4**, which leads to greater extension of the chains from the surface and a more hydrophobic surface with better transfer ratios. This effect is confirmed by transferring polymer **4** at an area per repeating unit of 145 Å^2, and the second downstroke transfer ratio was greater than 80%.

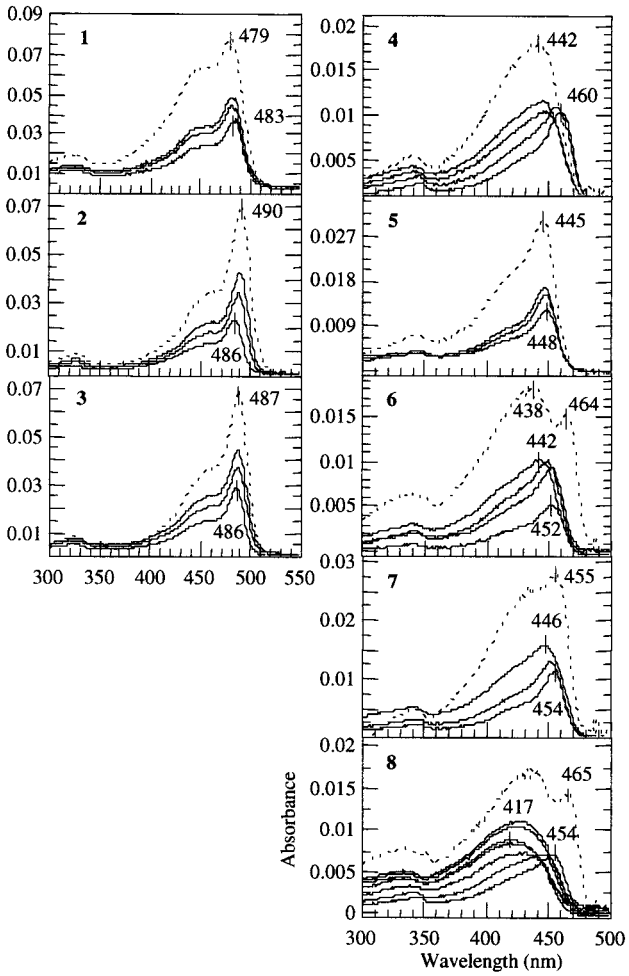

Figure 2. Surface pressure dependent in situ UV−vis spectra of polymers **1**−**8** at the air−water interface. The surface pressure was gradually increased from bottom solid line to top solid line (0, 18, 38 mN/m for polymer **1**; 0, 27, 40 mN/m for polymer **2**; 0, 20, 40 mN/m for polymer **3**; 0, 18, 27, 29 mN/m for polymer **4**; 0, 18, 30 mN/m for polymer **5**; 0, 6, 18, 27 mN/m for polymer **6**; 0, 18, 32 mN/m for polymer **7**; 0, 9, 15, 17, 23, 26, 30 mN/m for polymer **8**) until the monolayer folds into a multilayer (dashed line). The UV−vis spectra of polymers **2** and **4**−**8** are completely reversible upon cycles of compression and expansion.

The effects of the spatial arrangement on the electronic ground states of the polymers are revealed in the absorption spectra of the polymers' LB films (Figure 3) as well as in the in situ absorption spectra of polymers' Langmuir films at the air−water interface (Figure 2). As mentioned earlier, the edge-on structure gives crystalline aggregants at the onset. Therefore, Langmuir and LB films of the edge-on polymers show a new red-shifted absorption λ_{max} that is 30−40 nm to the red of the solution values. The spectra are unchanged when the monolayers fold into multilayers indicating that the aggregates are formed in a monolayer state. To further investigate the origin of the red-shifted absorption spectra of the edge-on polymers, three spin-cast films of polymer **1** in poly(methyl methacrylate) (PMMA) with different weight ratios from 10^{-3}/1 to 10^{-1}/1 (polymer **1**/PMMA) were prepared. As the concentration of polymer **1**

(19) Lucht, B. L.; Mao, S. S. H.; Tilley, T. D. *J. Am. Chem. Soc.* **1998**, *120*, 4354.
(20) Zhang, Q. T.; Tour, J. M. *J. Am. Chem. Soc.* **1997**, *119*, 9624.
(21) Miteva, T.; Palmer, L.; Kloppenburg, L.; Neher, D.; Bunz, U. H. F. *Macromolecules* **2000**, *33*, 652.

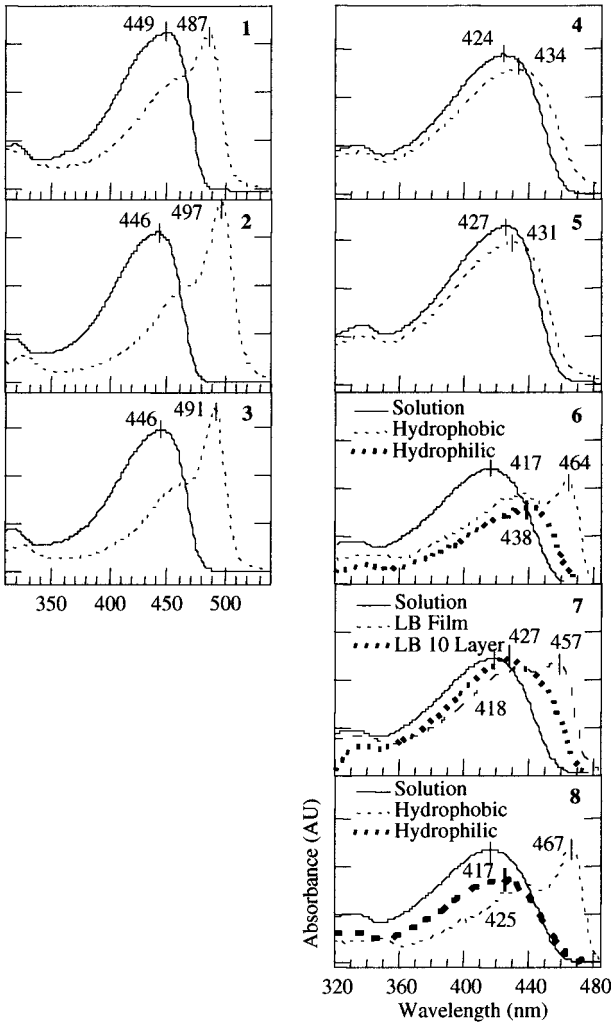

Figure 3. UV−vis spectra of polymers **1**−**8** in solution (solid line) and in LB films (dashed line). All LB films are monolayers on hydrophobic substrates unless otherwise noted.

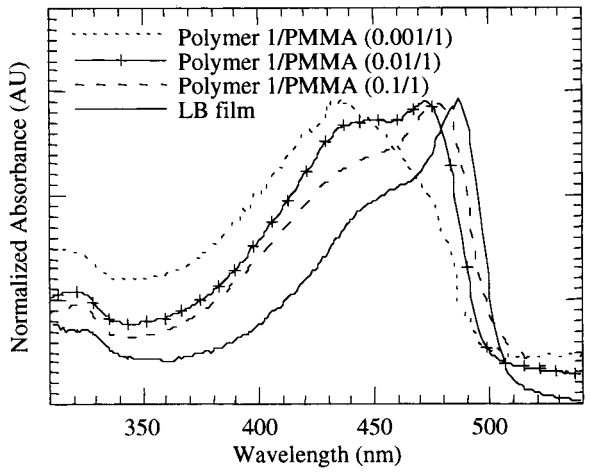

Figure 4. UV−vis spectra of polymer **1**/PMMA (weight ratio) spin-cast films.

increases in these films, the intensity of the higher wavelength absorption increases and is further red-shifted (Figure 4). These results are consistent with strong intermolecular π-stacking interactions promoted by the edge-on geometry. The broad peak at ca. 440 nm is similar to the solution spectra and represents a distribution of conjugation lengths. Therefore, the presence

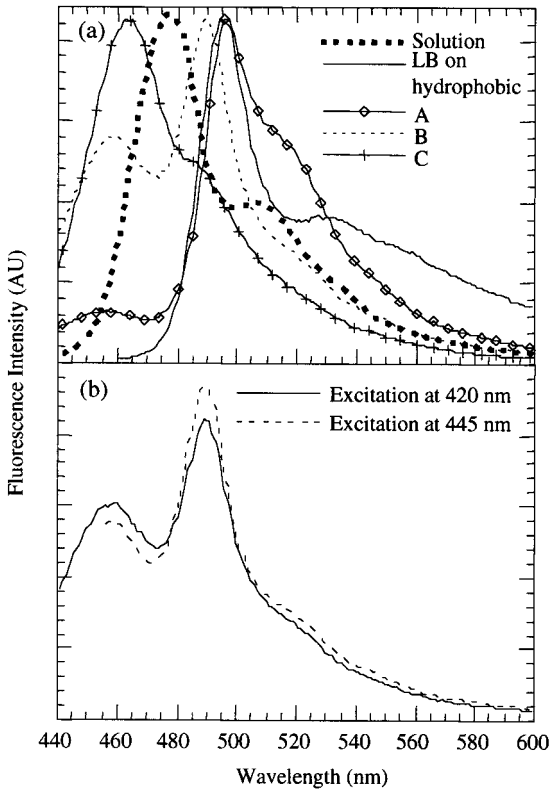

Figure 5. Fluorescence spectra of polymer **1** (a) normalized spectra in various environments, (b) in B at different excitation wavelength. The mass ratio of polymer **1**/PMMA in the spin-cast films is A = 10^{-1}/1, B = 10^{-2}/1, C = 10^{-3}/1, respectively.

of these two peaks in absorption spectra indicates the coexistence of monomer-like and aggregated regions in the film.[22]

Fluorescence spectra provide additional information about the relationship between the different polymer's excitation characteristics and film structures. The fluorescence spectra of monolayer LB films of the edge-on polymers **1**−**3** clearly demonstrate that all emission emanates from π-aggregated excited states. Figure 5a shows the fluorescence spectra of polymer **1** in solution, in spin-cast films with PMMA, and in monolayer LB films. As the concentration of polymer **1** in PMMA matrix increases and the aggregation band in absorption spectra increases (Figure 4), the short wavelength (solution-like) peak disappears, and a long wavelength peak grows in, thereby indicating the formation of π-aggregates. Excitation at different wavelengths resulted in the intensity redistribution between these two peaks (Figure 5b), proving that these two peaks belong to different excited and ground states. Therefore, we can exclude excimer species. In the case of polymer **1**, the fluorescence peak of π-aggregated PMMA films perfectly matched those of the LB film, and similar trends for polymers **2** and **3** were observed. Therefore, we conclude that the polymers **1**−**3** have both solution-like and π-aggregated regions in PMMA solid solutions, LB films, and Langmuir films, but all the fluorescence is emitted only from the aggregated states. This latter result is due to a fast energy migration from solution-like regions to the aggregated regions that have lower energy

(22) (a) Blatchford, J. W.; Gustafson, T. L.; Epstein, A. J.; VandenBout, D. A.; Kerimo, J.; Higgins, D. A.; Barbara, P. F.; Fu, D. K.; Swager, T. M.; MacDiarmid, A. G. *Phys. Rev. B* **1996**, *54*, R3683. (b) Blatchford, J. W.; Jessen, S. W.; Lin, L. B.; Gustafson, T. L.; Fu, D. K.; Wang, H. L.; Swager, T. M.; MacDiarmid, A. G.; Epstein, A. J. *Phys. Rev. B* **1996**, *54*, 9180.

Scheme 2

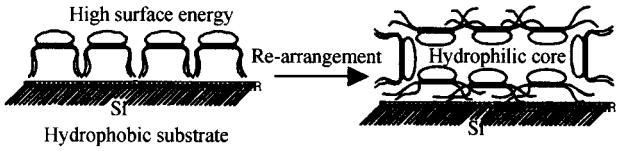

and act as excitation traps.[22] Therefore, the quantum yields of π-aggregates are low due to efficient self-quenching which is typical of most conjugated polymers (vide infra).

The face-on polymers have different absorption spectra depending on whether their LB films are transferred onto a hydrophobic or a hydrophilic substrate (Figure 3). These results are in accord with our previous investigations and are related to structural differences of the transferred films. As we previously reported for polymer **4**, monolayers of other face-on polymers **5**−**8** on a hydrophilic substrate also have a smooth flat surface.[13] This structure is stable due to favorable strong anchoring interactions between the polar surface and the oxygen moieties in the polymer. In contrast, monolayers of the face-on polymers on a weak anchoring hydrophobic substrate reconstruct into "nanofibrils" to relieve the high surface energy of the polar macrocycles as described in Scheme 2 and shown in Figure 6.[13] Because these monolayers cannot have π-aggregation when they are tightly bound (anchored) to hydrophilic substrates, no aggregation peaks are observed in their UV−vis spectra. However, for nanofibriled monolayer films on hydrophobic substrates, the formation of an aggregation peak depends on the structure of the hydrophilic repeating group. Macrocycles containing polymers **4** and **5** display solution-like absorption spectra without any aggregation peak after assembly into nanofibrils. The spectra of **4** and **5** are slightly red-shifted from those in solution due to an increase in conjugation length imposed by the surface. The lack of π-aggregation is due to the macrocycles in **4** and **5** that by virtue of their structure prevent direct interpolymer interactions between the conjugated aromatic rings. It follows that the folded Langmuir or multilayer LB films of **4** and **5** did not show the π-aggregation peak.

Polymers **6** and **8** have acyclic polar residues, and the in situ absorption spectra showed π-aggregation peaks after the Langmuir monolayers are folded into multilayers (Figure 2). Because of the reversible nature of the PA isotherm, the π-aggregation does not persist upon removal of the surface pressure. The absorption spectra of these polymer nanofibril monolayers on hydrophobic substrates also show the additional π-aggregation peaks at longer wavelengths, 464 and 467 nm, respectively, values about 50 nm red to their solution λ_{max} (Figure 3). Interestingly, the extent of π-aggregation in their nanofibril LB

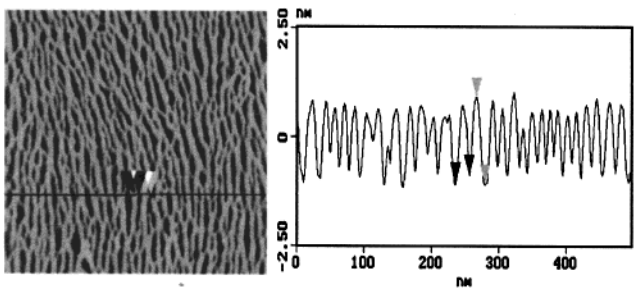

Figure 6. Atomic force microscope image (500 × 500 nm) of a nanofibril monolayer LB film of polymer **4** and a sectional profile across the nanofibrils. Nanofibrils are aligned along the dipping direction.

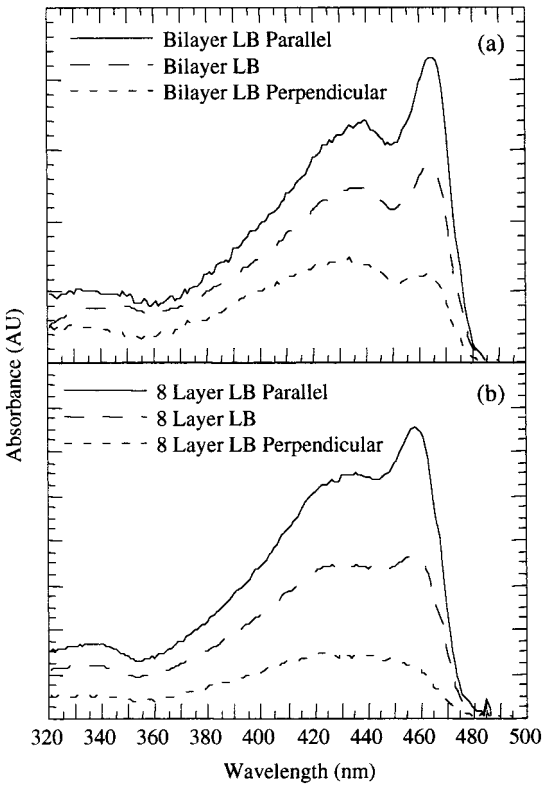

Figure 7. Polarized UV−vis spectra of (a) polymer **6** and (b) polymer **7**.

films is responsive to its environment. Dipping a nanofibril monolayer of **6** with a π-aggregation peak in water produces a solution-like UV−vis spectra. The π-aggregation peak is then reestablished with drying. Because the cores of the nanofibrils are hydrophilic (Scheme 2), water dilates the nanofibrils, thereby diminishing intermolecular interactions between polymers. Consistently, hydrophobic solvents are not absorbed into the fibrils, and the same film retains the aggregation peak upon dipping in hexane.

The polarized UV−vis spectra of nanofibril monolayer films of polymers **6** and **7** in Figure 7 provide additional information about the aggregate regions. For polymer **6**, the aggregation peak at 464 nm in the parallel polarized UV−vis spectrum along the polymer alignment direction is of greater intensity than the solution-like peak at 438 nm. In contrast, the intensity of the aggregation peak in perpendicularly polarized spectra is less intense relative to the solution-like peak, indicating that the aggregate regions are better aligned along the dipping direction than are the nonaggregated regions. This result is intuitive because coincident alignment of polymer chains promotes aggregation. Even though it lacks macrocycles, nanofibrils of polymer **7** do not form π-aggregation peaks in absorption spectrum. It appears that the hydroxyl groups play an important role in reducing intermolecular interaction in the nanofibrils by strongly holding water molecules in the cores of the nanofibrils. This explanation is also supported by the behavior of **6** and **8** that form π-aggregates in dry nanofibrils, but then deaggregate when immersed in water. Folded Langmuir films of polymer **7** did not show additional π-aggregation peaks either (Figure 2). However, multilayer LB films of polymer **7** display a π-aggregation peak that increased with dehydration in a vacuum.

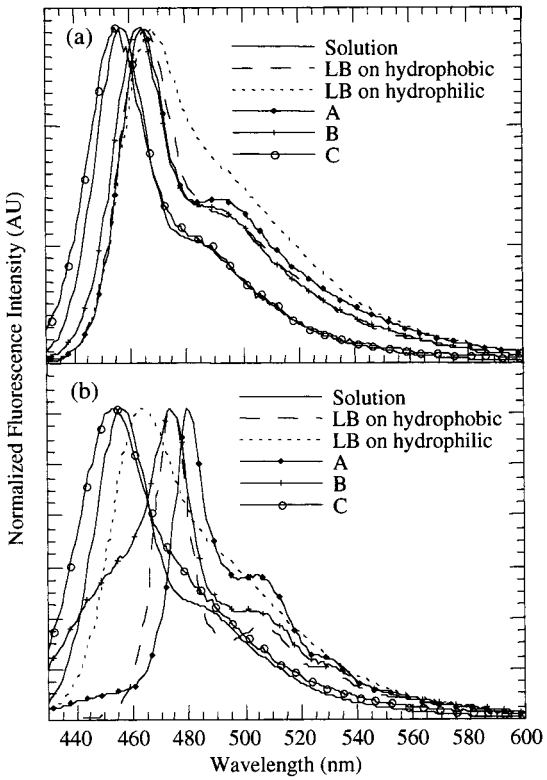

Figure 8. Fluorescence spectra of polymers (a) **4** and (b) **8**. The mass ratio of polymer/PMMA in the spin-cast films is A = 10^{-1}/1, B = 10^{-2}/1, C = 10^{-3}/1, respectively.

As shown in Figure 7b, these multilayer films show π-aggregate absorptions that are polarized along the direction of the polymer alignment.

Structural differences in monolayer LB films of the face-on polymers also affect emission spectra. The nanofibril monolayers of polymers **6** and **8** on hydrophobic substrates, with an aggregation peak in their absorption spectra, have structured fluorescence spectra with three peaks. On the other hand, the UV−vis spectra of the nanofibriled monolayers of polymers **4**, **5**, and **7** on hydrophobic substrates do not show aggregation, and their fluorescence spectra are less structured. In the case of polymer **7**, we observed that the aggregation peak increased when the number of layers in the LB films increased, indicating a gradual increase of intermolecular interactions. We observed the same effect of intermolecular interactions on the fluorescence spectra of multilayer films of polymer **7**. From a relatively featureless solution-like shape for a monolayer film, the spectra developed structure as the number of layers increased. Aggregation and highly ordered segments are mutually reinforcing and produce narrowed and structured fluorescence spectra. Energy migration to the aggregates also facilitates the band narrowing by reducing the contribution of solution-like fluorescence.

Fluorescence studies of spin-cast films of these polymers in PMMA solid solutions are consistent with the UV−vis analysis, that polymers **4**, **5**, and **7** do not form aggregates, whereas polymers **6** and **8** do. Figure 8 shows fluorescence spectra of polymers **4** and **8** in solution, in spin-cast films with PMMA, and in LB films on both hydrophobic and hydrophilic substrates. As the concentration of polymer **4** in a spin-cast film with PMMA increased, the emission λ_{max} undergoes slight red shifts (Figure 8a). However, polymers with a tendency to aggregate showed significant spectral changes. In Figure 8b, increasing concentrations of polymer **8** in spin-cast films with PMMA induced the evolution of fluorescence spectra from solution-like behavior to those characteristics of π-aggregation. The fluorescence spectrum of a spin-cast film at a low concentration (10^{-2}/1, polymer **8**/PMMA) clearly showed a solution-like shoulder that decreases at higher concentrations of polymer **8**.

Table 1. Photophysical Data of the Polymers[a]

polymer	optimized $A_{\parallel}/A_{\perp}$	fluorescence λ_{max} (nm) in solution	fluorescence λ_{max} (nm) in LB film	quantum yield (Φ_F) in solution (A)	quantum yield (Φ_F) in LB film (B)	Φ_F ratio (B/A)
1	3.0	476	493	0.43	0.002	0.005
2	3.6	471	505	0.34	0.007	0.02
3	3.0	474	500	0.36	0.01	0.03
4	6.3	457	465	0.54	0.19	0.35
5	5.0	456	459	0.41	0.17	0.41
6	5.5	455	472	0.46	0.14	0.30
7	4.3	456	466	0.53	0.17	0.32
8	1.4	457	474	0.44	0.10	0.23

[a] See Experimental Section for the detailed information. LB films in this table were monolayer films on hydrophobic substrates.

Interpolymer Effects on Fluorescence Quantum Yield of Polymer Films. Table 1 shows the fluorescence quantum yields of the polymers in chloroform solution and in monolayer LB films on a hydrophobic substrate, and the ratio thereof (i.e., quantum yield in LB films/quantum yield in solution). The fluorescence quantum yields of the polymers in solution are similar and range from 0.34 to 0.54. The organizations have a larger effect, and monolayer LB films of face-on polymers have at least an order of magnitude higher quantum yield as compared to those of edge-on polymers.

Generally, monolayers on hydrophilic substrates have much smaller fluorescence quantum yields than monolayers on hydrophobic substrates. For example, the quantum yields of monolayers of polymers **1**, **4**, and **6** on a hydrophilic substrate are ~0.0015, 0.05, and 0.05, respectively. The lower quantum yields of the monolayers on hydrophilic substrates may arise from stronger interactions between the polymers' hydrophilic groups and the substrates.

By comparing the ratio of quantum yield in LB films/quantum yield in solution, we can see the influence of intermolecular interactions on the quantum yield. First, the strong π-aggregating edge-on polymers display self-quenching and extremely low quantum yields. Second, the face-on polymers, which are devoid of strong π-aggregates, experience varying degrees of interpolymer interactions in nanofibrils. The ratio of quantum yield in LB films/quantum yield in solution has a tendency to increase as intermolecular interactions in nanofibrils decrease. Macrocycles of polymers **4** and **5** reduce intermolecular interactions in the nanofibrils significantly, resulting in the best ratio of quantum yield in LB films/quantum yield in solution.

Conclusions

We have demonstrated control of the spatial arrangement of PPEs by designed chemical structures and the LB method. This precise control of the spatial arrangement of conjugated polymers allowed us to elucidate aggregation mechanisms and the effect of π-aggregation on the spectroscopic properties of conjugated polymers. Through extensive structure−property correlations, we have firmly established spectroscopic features associated with nonaggregated polymers with various conjuga-

tion lengths. In well-defined LB films and various solid solutions, we demonstrated that strong π-aggregates present in fluorescent polymer thin films result in quenching due to efficient energy migration from nonaggregated regions to the aggregated ones. Intermolecular interactions in nanofibrils also affect the photophysical properties of the polymers. Macrocycles attached to the polymer backbone significantly reduce intermolecular interactions in the solid state, thereby increasing quantum yield relative to polymers without macrocycles. In well-defined monolayer LB films, orders of magnitude different quantum yields were obtained depending on spatial arrangement of polymers even though the solution quantum yields are similar to each other. These comprehensive results provide important design principles for fabricating highly luminescent polymer films. Because chemical modification can give surfactant character to other conjugated polymers, this method is potentially applicable to general conjugated polymers.

Experimental Section

General. Air- and moisture-sensitive reactions were carried out in flame-dried glassware using standard Schlenk-line or drybox techniques under an inert atmosphere of dry argon. All chemicals used were of reagent grade and were purchased from Aldrich unless otherwise noted. Anhydrous toluene was used from Aldrich Kilo-lab metal cylinders. CH_2Cl_2 and THF were used directly from Aldrich Sure-seal bottles. Diisopropylamine was distilled over solid KOH pellets and degassed by three freeze−pump−thaw cycles. Tetrakis(triphenylphosphine)-palladium (0) and *trans*-dichlorobis(triphenylphosphine)-palladium (II) were purchased from Strem chemicals and used as received. (Trimethylsilyl)acetylene was purchased from Farchan Laboratories and used as received. ^{1}H and ^{13}C NMR spectra were taken in $CDCl_3$ with ^{1}H chemical shifts reported relative to internal tetramethylsilane (0.00 ppm) and ^{13}C chemical shifts reported relative to $CDCl_3$ (77.00 ppm). 2,5-Diiodo-4-decyloxyanisole,[13] 2,5-diethynyl-4-decyloxyanisole,[13] 1,4-diiodo-2,5-dihydroxybenzene,[23] 1,4-bis (*N*,*N*-dioctylcarbamoyl)-2,5-diiodobenzene,[23] 1,4-bis[2-(2-hydroxyethoxy)ethoxy]-2,5-diethynylbenzene,[6] and polymers **1**,[13] **3**,[4d] **4**,[23] and **6**[12] were synthesized according to the literature procedures.

Polymer molecular weights were determined with a Hewlett-Packard 1100 series HPLC equipped with a PLgel mixed-C column (5 μ) using THF as the mobile phase at a rate of 1 mL/min. Gel permeation chromatography (GPC) measurements were made relative to monodisperse polystyrene standards purchased from Polymer Laboratories. This technique may give relative molecular weights higher than the actual values for rigid-rod polymers. The overestimate of the molecular weight of PPEs by GPC is largest for low molecular weight samples, and high molecular weight samples have a very modest correction.[24] LB thin films were prepared on a 601 M LB trough equipped with vertical dipping mechanism from NIMA Technology, Ltd., using purified water (18 MΩ) from a Barnstead Nanopure system. Substrates were 18 × 18 mm glass microscope cover slides treated according to the literature.[13] UV−vis spectra were obtained on a Hewlett-Packard 8453 diode array spectrophotometer. To collect UV−vis spectra versus surface pressure of polymers' films at the air−water interface, a LB trough with a window was placed in a vertically rotated UV spectrophotometer. Fluorescence spectra were measured at room temperature using a SPEX Fluorolog-τ2 spectrofluorometer. Fluorescence quantum yields in chloroform solutions and monolayer LB films were determined relative to equiabsorbing quinine sulfate solution ($\sim 10^{-6}$ M in 1 N H_2SO_4, $\Phi_F = 0.55$)[25] and spin-cast films of $\sim 10^{-3}$ M 9,10-diphenylanthracene in PMMA ($\Phi_F = 0.83$),[5d] respectively, by using the equation $\Phi_F = [(A_s F_u n_u^2)/(A_u F_s n_s^2)]\Phi_s$,[26] where subscripts s and u refer to standard and unknown samples, respectively. A is the optical density at the excitation wavelength, F is the integrated area of the fluorescence spectrum, and n is the refractive index. We assumed that the refractive indices of LB films are the same and the refractive index of quinine sulfate solution is the same as pure water.

Polymer 2. A 10 mL Schlenk flask equipped with a stir bar was charged with 1-((triethylene glycol monomethyl ether)oxy)-4-decyloxy-2,5-diiodobenzene (73.1 mg, 0.11 mmol, 1 equiv), 1-((triethylene glycol monomethyl ether)oxy)-4-decyloxy-2,5-diethynylbenzene (**9**) (51.6 g, 0.11 mmol, 1.03 equiv), and copper(I)iodide (3.9 mg, 20.5 μmol, 0.07 equiv). The flask was placed under argon, and tetrakis(triphenylphosphine)-palladium (0) (8 mg, 6.92 μmol, 0.18 equiv) was added under a nitrogen atmosphere. Toluene (3.0 mL) and diisopropylamine (DIPA) (1.25 mL, 8.91 mmol, 79 equiv) were successively added by syringe, and the mixture was stirred at room temperature for 30 min. As the mixture became viscous, toluene (2 mL) was added, after which the mixture was heated to 60 °C for 24 h. The polymer solution was then precipitated in methanol, filtered, and rinsed with hot methanol, giving polymer **2** as an amorphous orange solid. ^{1}H NMR (300 MHz, $CDCl_3$): δ 7.06 (s, 1H), 7.01 (s, 1H), 4.24 (br m, 2H), 4.04 (br m, 2H), 3.92 (br m, 2H), 3.78 (br m, 2H), 3.62 (br m, 4H), 3.51 (br m, 2H), 3.35 (br m, 3H), 1.86 (br m, 2H), 1.64−1.10 (br m, 14H), 0.87 (t, J = 6.9 Hz, 3H). GPC: M_n = 55 900; PDI = 2.9.

2,5-Diiodo-*p*-phenylene-20-crown-6. This compound was a side product of a reaction. Flash chromatography (20% ethyl acetate/5% methanol/75% hexane) afforded a white solid. ^{1}H NMR (250 MHz, $CDCl_3$): δ 7.32 (s, 2H), 4.41−4.21 (m, 4H), 3.88−3.72 (m, 4H), 3.60−3.53 (m, 8H), 3.33 (s, 4H). ^{13}C NMR (125 MHz, $CDCl_3$): δ 153.43, 124.57, 87.23, 71.68, 70.99, 70.89, 70.51. Anal. Calcd for $C_{16}H_{22}I_2O_6$: C, 34.06; H, 3.93. Found: C, 34.05; H, 4.02.

2,5-Diethynyl-*p*-phenylene-20-crown-6 (10). A 50 mL Schlenk flask equipped with a stir bar was charged with 2,5-diiodo-*p*-phenylene-20-crown-6 (0.564 g, 1 mmol, 1 equiv), *trans*-dichlorobis(triphenylphosphine)-palladium (II) (14 mg, 19.9 μmol, 0.02 equiv), and copper(I) iodide (5.7 mg, 29.9 μmol, 0.03 equiv). The flask was placed under argon, and then toluene (10 mL) and diisopropylamine (20 mL, 0.14 mol, 130 equiv) were successively added. The orange solution was treated with (trimethylsilyl)acetylene (TMSA) (0.31 mL, 2.2 mmol, 2.2 equiv) and stirred at 70 °C for 48 h. The solvent was removed in vacuo, and the residue was dissolved in CH_2Cl_2. The black mixture was filtered through a 1 in. plug of silica gel and eluted using ethyl acetate. The filtrate was removed in vacuo to yield a black oil that was chromatographed (10% CH_2Cl_2/25% ethyl acetate/70% hexane, R_f = 0.24) to afford 2,5-((trimethylsilyl)ethynyl)-*p*-phenylene-20-crown-6 as a yellow solid (0.34 g, 67%).

A 100 mL two-necked round-bottomed flask equipped with a stir bar was charged with 2,5-((trimethylsilyl)ethynyl)-*p*-phenylene-20-crown-6 (0.24 g, 0.48 mmol, 1 equiv) and methanol (10 mL). The flask was capped and argon bubbled through the solution for 45 min. Tetrabutylammonium fluoride hydrate (TBAF) (0.30 g, 1.14 mmol, 2.4 equiv) was then added to the flask under argon, and the mixture was stirred at room temperature for 12 h. The red solution was then concentrated in vacuo, and the residue was partitioned between CH_2Cl_2 (100 mL) and water (50 mL). The organic layer was washed with saturated aqueous NaCl (50 mL), and then dried ($MgSO_4$), and concentrated in vacuo. Flash chromatography (50% CH_2Cl_2/45% hexane/5% methanol, R_f = 0.25) afforded **10** (0.13 g, 77%) as a light yellow solid. ^{1}H NMR (250 MHz, $CDCl_3$): δ 7.11 (s, 2H), 4.46−4.26 (m, 4H), 3.81−3.78 (m, 4H), 3.67−3.52 (m, 8H), 3.38 (s, 4H), 3.34 (s, 2H). ^{13}C NMR (75 MHz, $CDCl_3$): δ 154.33, 119.80, 114.04, 82.54, 80.30, 71.72, 71.00, 70.95, 70.88, 69.75 ppm. HR-MS: calcd for $C_{20}H_{24}O_6$ (M^+), 360.1573; found, 360.1567.

Polymer 5. A 10 mL flame-dried Schlenk flask equipped with a stir bar was charged with 1,4-bis (*N*,*N*-dioctylcarbamoyl)-2,5-diiodo-

(23) Zhou, Q.; Swager, T. M. *J. Am. Chem. Soc.* **1995**, *117*, 7017.
(24) Cotts, P. M.; Swager, T. M.; Zhou, Q. *Macromolecules* **1996**, *29*, 7323.
(25) Demas, J. N.; Crosby, G. A. *J. Phys. Chem.* **1971**, *75*, 991.
(26) Eaton, D. F. *Pure Appl. Chem.* **1988**, *60*, 11

benzene (86.5 mg, 100 μmol, 1 equiv), 2,5-diethynyl-*p*-phenylene-20-crown-6 (**10**) (36 mg, 99.9 μmol, 1 equiv), and copper(I)iodide (2.3 mg, 12 μmol, 0.12 equiv). The flask was placed under argon, and tetrakis-(triphenylphosphine)palladium (0) (8.1 mg, 7 μmol, 0.07 equiv) was added under a nitrogen atmosphere. Toluene (1 mL) and diisopropylamine (1.12 mL, 8 mmol, 80 equiv) were successively added by syringe, and the mixture was stirred at 70 °C for 60 h. The cooled polymer solution was precipitated in methanol, filtered, and rinsed with warm methanol. After drying under high vacuum, polymer **5** was obtained as a brown solid. ^{1}H NMR (300 MHz, $CDCl_3$): δ 7.48 (s, 2H), 7.04 (s, 2H), 4.30 (br m, 4H), 3.84 (m, 4H), 3.70−3.40 (br m, 10H), 3.37 (m, 4H), 3.20 (br m, 6H), 1.70−1.03 (m, 48H), 0.86 (m, 12H). GPC: M_n = 56 000; PDI = 2.5.

1,4-Bis[2-(2-hydroxyethoxy)ethoxy]-2,5-diethynylbenzene (11). 1,4-Bis[2-(2-hydroxyethoxy)ethoxy]-2,5-diiodobenzene was combined with *trans*-dichlorobis(triphenylphosphine)-palladium (II) (39 mg, 56 μmol, 0.03 equiv) and copper(I)iodine (21 mg, 110 μmol, 0.06 equiv) in a flame-dried flask equipped with a stir bar. The flask was evacuated and back filled with argon three times. The solids were dissolved/suspended in toluene (25 mL) and diisopropyle amine (652 μL). The (trimethylsilyl)actylene (0.580 mL, 4.1 mmol, 2.2 equiv) was then added, and the reaction was stirred and heated to 60 °C for 20 h. Once the reaction was cooled to room temperature, saturated ammonium chloride solution was added, and the biphasic mixture was stirred for 30 min. The layers were then separated after dilution with ether. The organic layer was washed four times with saturated ammonium chloride solution, dried with magnesium sulfate, filtered, and concentrated to give a dark brown oil that was chromatographed on silica gel (50% hexane/50% ethyl acetate).

The bistrimethylsiylacetylene (850 mg, 1.8 mmol, 1 equiv) was deprotected by reaction with aqueous potassium hydroxide (200 mg, 3.6 mmol, 2 equiv; dissolved in 1 mL of DDI water) in degassed THF (17 mL) and methanol (13.3 mL). The solution was stirred for 48 h. The reaction was then poured into 50 mL of ether. The organic layer was separated and washed with water three times (40 mL). The organic layer was dried with magnesium sulfate and concentrated to provide an off-white solid that was recrystallized from ethanol to provide **11**. ^{1}H NMR (300 MHz, $CDCl_3$): δ 7.00 (s, 2H), 4.16 (m, 4H), 3.88 (m, 4H), 3.74 (m, 4H), 3.69 (m, 4H), 3.36 (s, 2H), 2.21 (br s, 2H). ^{13}C NMR (75 MHz, $CDCl_3$): δ 153.76, 118.03, 113.44, 82.99, 79.38, 72.53, 69.39, 69.22, 61.79 ppm. HR-MS: calcd for $C_{18}H_{22}O_6$ (M^+), 334.1416; found, 334.1424.

Polymer 7. A 10 mL Schlenk flask equipped with a stir bar was charged with 1,4-bis[2-(2-hydroxyethoxy)ethoxy]-2,5-diethynylbenzene (**11**) (30 mg, 91.3 μmol, 1.05 equiv) and 1,4-bis (*N*,*N*-dioctylcarbamoyl)-2,5-diiodobenzene (75 mg, 87 μmol, 1 equiv). Tetrakis-(triphenylphosphine)palladium (0) (3.1 mg, 4.35 μmol, 0.05 equiv) and copper(I) iodine were added to the flask under a nitrogen atmosphere. The flask was then evacuated and back filled with argon three times before adding toluene (1.5 μL) and diisopropylamine (500 μL) via cannula. The reaction was stirred while maintaining the temperature at 60 °C for 48 h. The reaction was cooled before diluting with methylene chloride and subsequent washing with ammonium hydroxide. The organic layer was concentrated to a yellow film that was redissolved in methanol and precipitated with water. After drying, polymer **7** was obtained as a fluorescent green-yellow solid. ^{1}H NMR (300 MHz, $CDCl_3$): δ 7.51 (s, 2H), 6.95 (s, 2H), 4.14 (br s, 4H), 3.90 (br s, 6H), 3.82−3.52 (br m, 8H), 3.16 (br s, 6H), 2.19 (br), 1.82−1.02 (m, 48H), 0.86 (m, 12H). GPC: M_n = 51 600; PDI = 3.8.

Polymer 8. A 10 mL flame-dried Schlenk flask equipped with a stir bar was charged with 1,4-bis (*N*,*N*-dioctylcarbamoyl)-2,5-diiodobenzene (86.5 mg, 100 μmol, 1 equiv), 1-((triethylene glycol monomethyl ether)oxy)-4-decyloxy-2,5-diethynylbenzene (**9**) (45.8 mg, 103 μmol, 1.03 equiv), and copper(I)iodide (2.3 mg, 12 μmol, 0.12 equiv). The flask was placed under argon, and tetrakis-(triphenylphosphine)-palladium (0) (8.1 mg, 7 μmol, 0.07 equiv) was added under a nitrogen atmosphere. Toluene (2 mL) and diisopropylamine (1.12 mL, 8 mmol, 80 equiv) were successively added by syringe, and the mixture was stirred at 70 °C for 43 h. The cooled polymer solution was precipitated in methanol, filtered, and rinsed with warm methanol. After drying under high vacuum, polymer **8** was obtained as a brown solid. ^{1}H NMR (300 MHz, $CDCl_3$): δ 7.46 (s, 2H), 6.92 (s, 1H), 6.84 (s, 1H), 4.16 (br s, 2H), 4.00−3.80 (m, 4H), 3.78 (m, 2H), 3.68 (m, 6H), 3.56 (m, 2H), 3.38 (s, 3H), 3.18 (br s, 6H), 1.80−1.03 (m, 64H), 0.89 (m, 15H) ppm. GPC: M_n = 16 700; PDI = 2.4.

Acknowledgment. The authors thank the Office of Naval Research, the Center for Materials Science and Engineering at MIT (NSF MRSEC), and Draper Lab for generous financial support, and Mr. Davide L. Simone for providing 2,5-diiodo-*p*-phenylene-20-crown-6. D.T.M. thanks the National Institute of Health for a postdoctoral fellowship through NISMS.

JA0200600